Future changes in boreal winter ENSO teleconnections in a large ensemble of high-resolution climate simulations

Nathaniel C. Johnson[1*], Andrew T. Wittenberg[1], Anthony J. Rosati[1,2], Thomas L. Delworth[1], William Cooke[1]

[1]Geophysical Fluid Dynamics Laboratory, National Oceanic and Atmospheric Administration, Princeton, NJ, USA

[2]University Corporation for Atmospheric Research, Boulder, CO, USA

Supplementary Material

1 Supplementary Figures

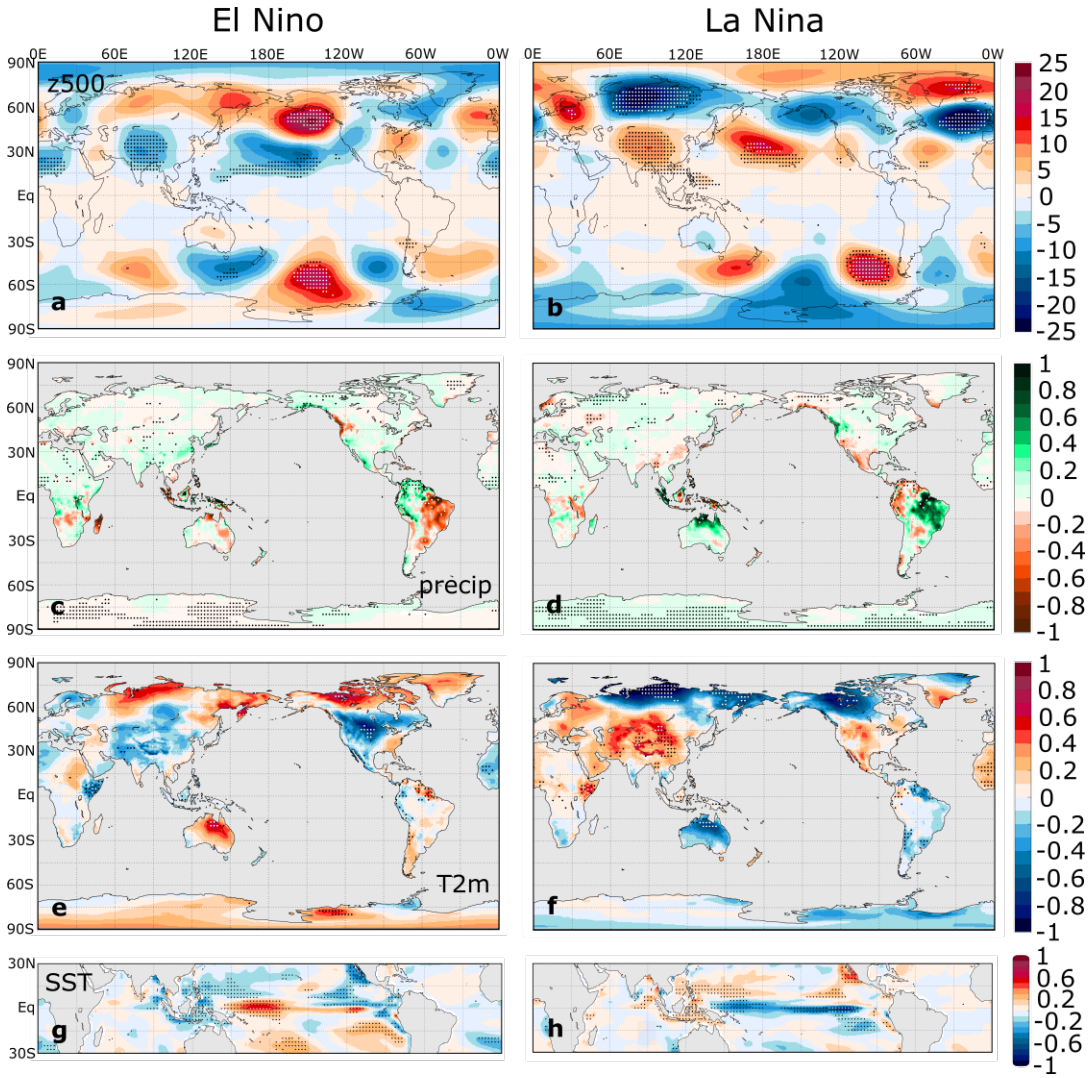

Supplementary Figure 1. Difference between SPEAR and observational (SPEAR minus observational) DJF (left) El Niño and (right) La Niña composites of (a,b) 500 hPa geopotential height (m), (c,d) precipitation (mm d^{-1}), (e,f) T2m (°C), and (g,h) SST (°C) anomalies for the 1951-2020 period. Stippling indicates that the observational composite is below the 5th percentile or above the 95th percentile of the SPEAR composites, as determined from the distribution of the 30 ensemble members.

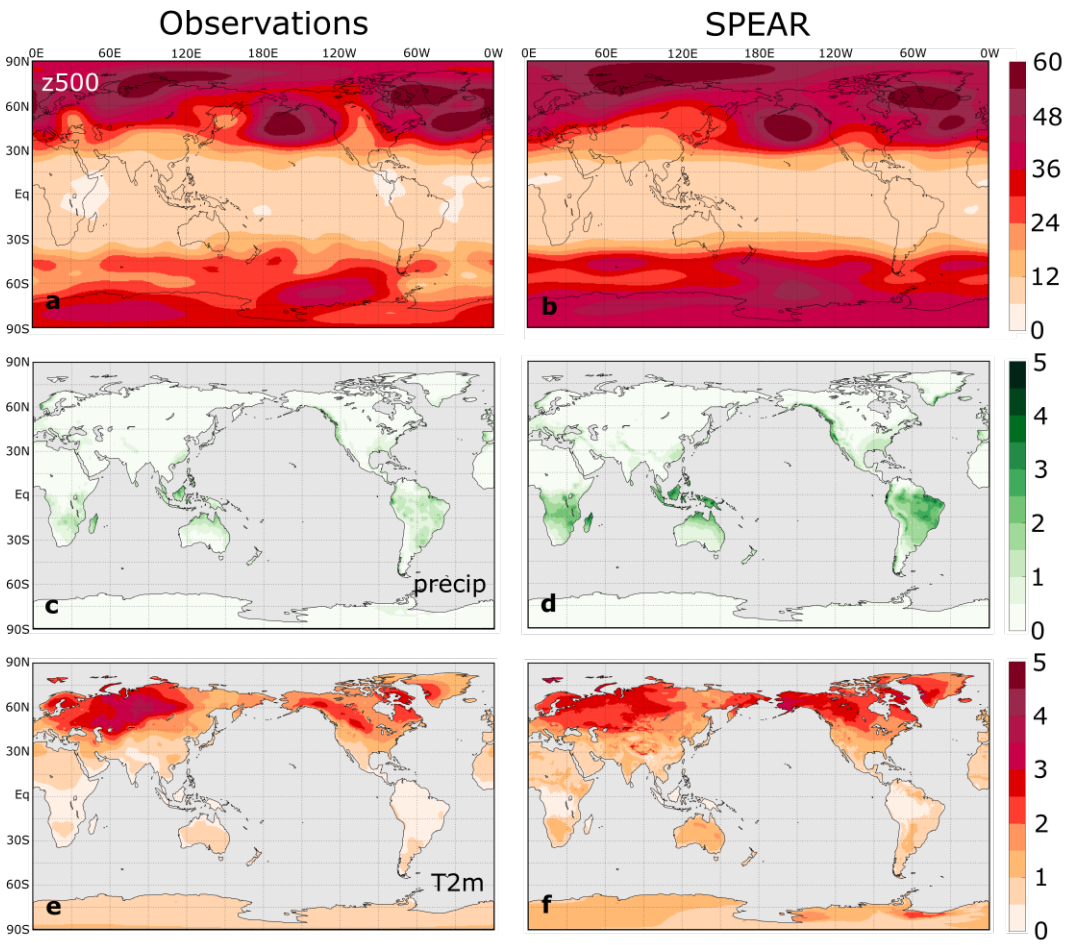

Supplementary Figure 2. Standard deviations of DJF mean (a,b) 500 hPa geopotential height (m), (c,d) precipitation (mm d^{-1}), and (e,f) T2m (°C) anomalies for all (left) observational and (right) SPEAR for all El Niño winters from 1951-2020.

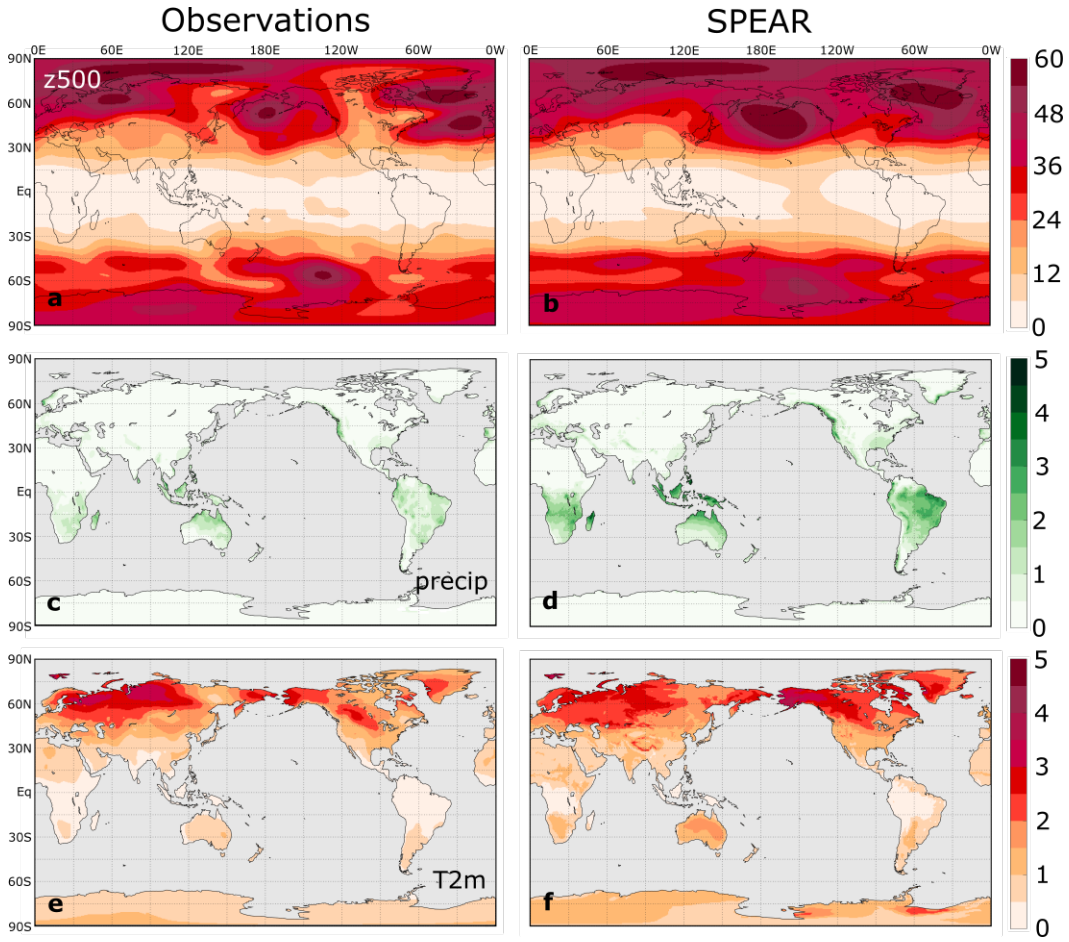

Supplementary Figure 3. As in Supplementary Fig. 2 but for La Niña instead of El Niño.

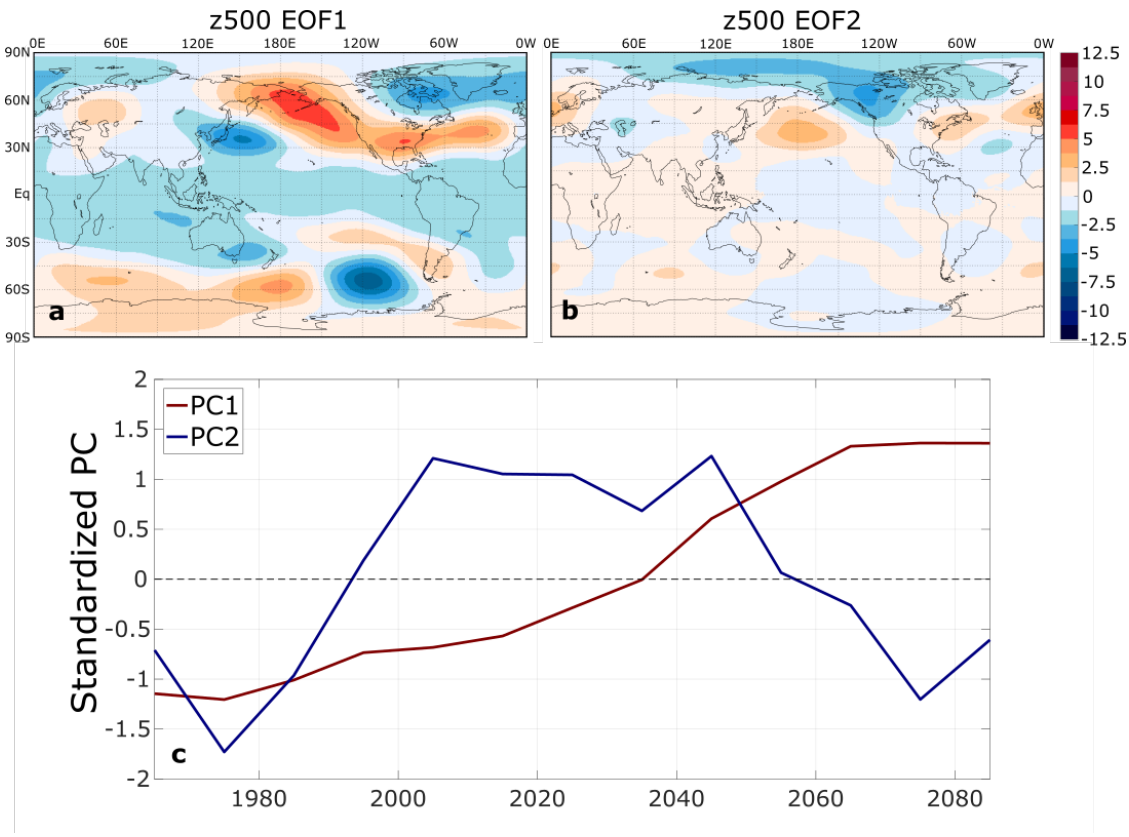

Supplementary Figure 4. The leading EOFs of Northern Hemisphere DJF ensemble mean z500 composite anomalies, as in Fig. 5, but for La Niña instead of El Niño. The two leading EOFs explain 69.1% and 17.5% of the z500 composite variance, respectively.

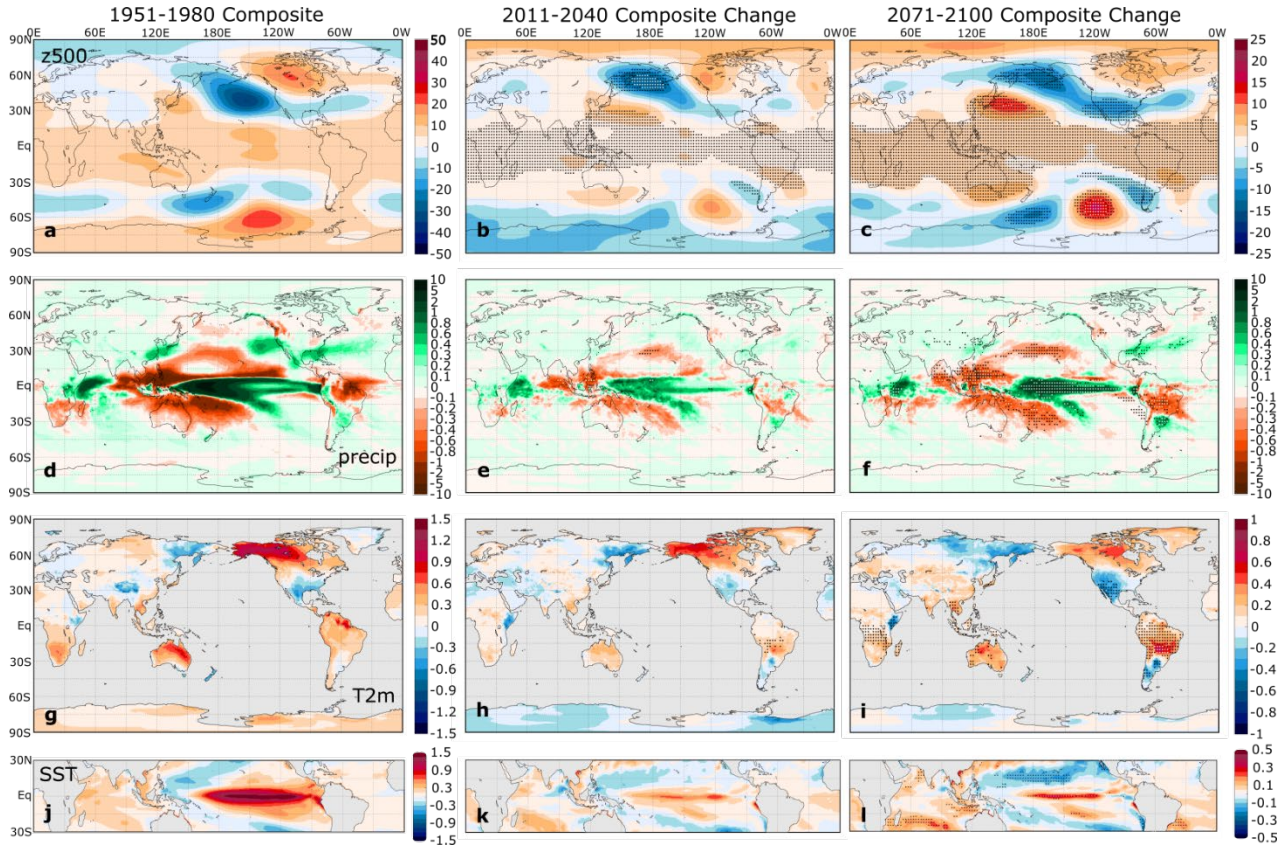

Supplementary Figure 5. Ensemble mean SPEAR DJF El Niño composites, as in Fig. 3, but for the SSP2-4.5 instead of the SSP5-8.5 scenario.

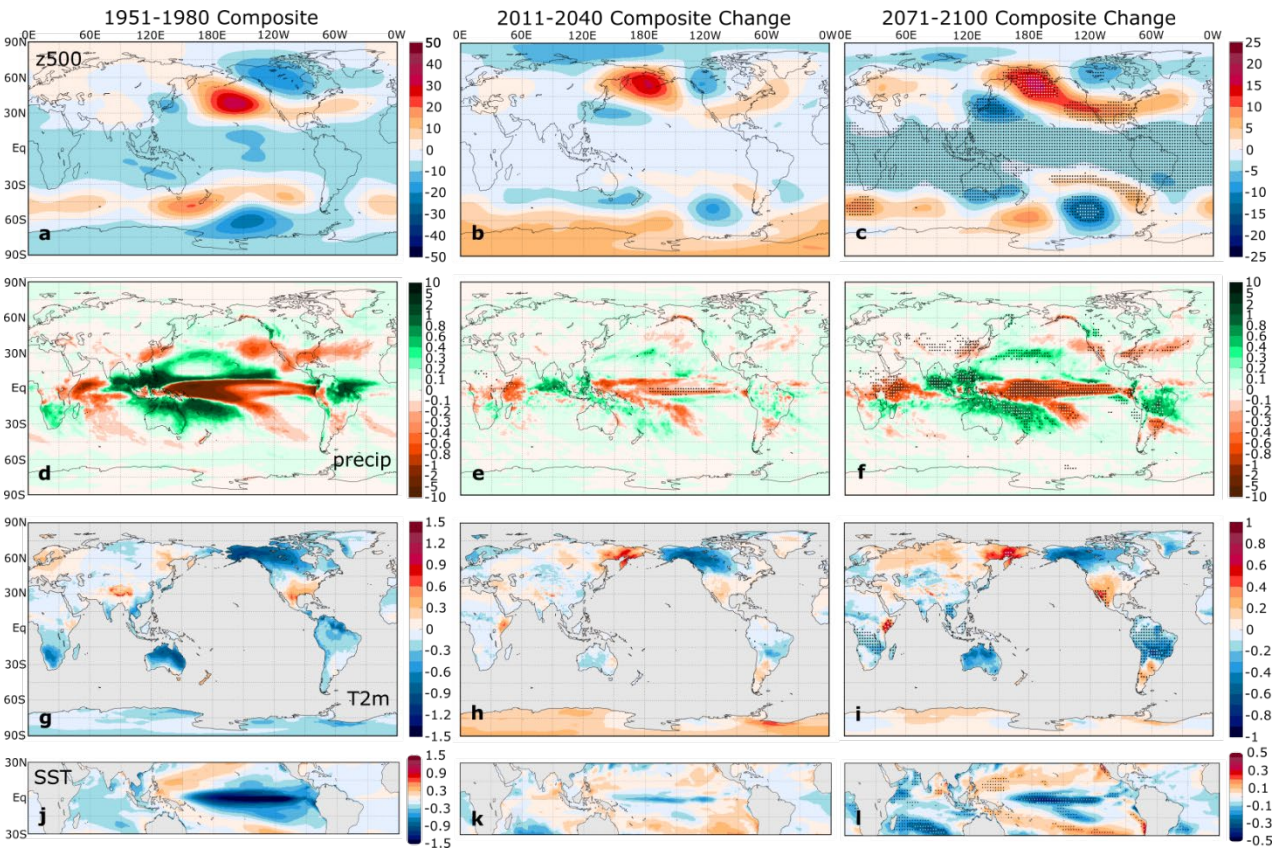

Supplementary Figure 6. Ensemble mean SPEAR DJF La Niña composites, as in Fig. 4, but for the SSP2-4.5 instead of the SSP5-8.5 scenario.

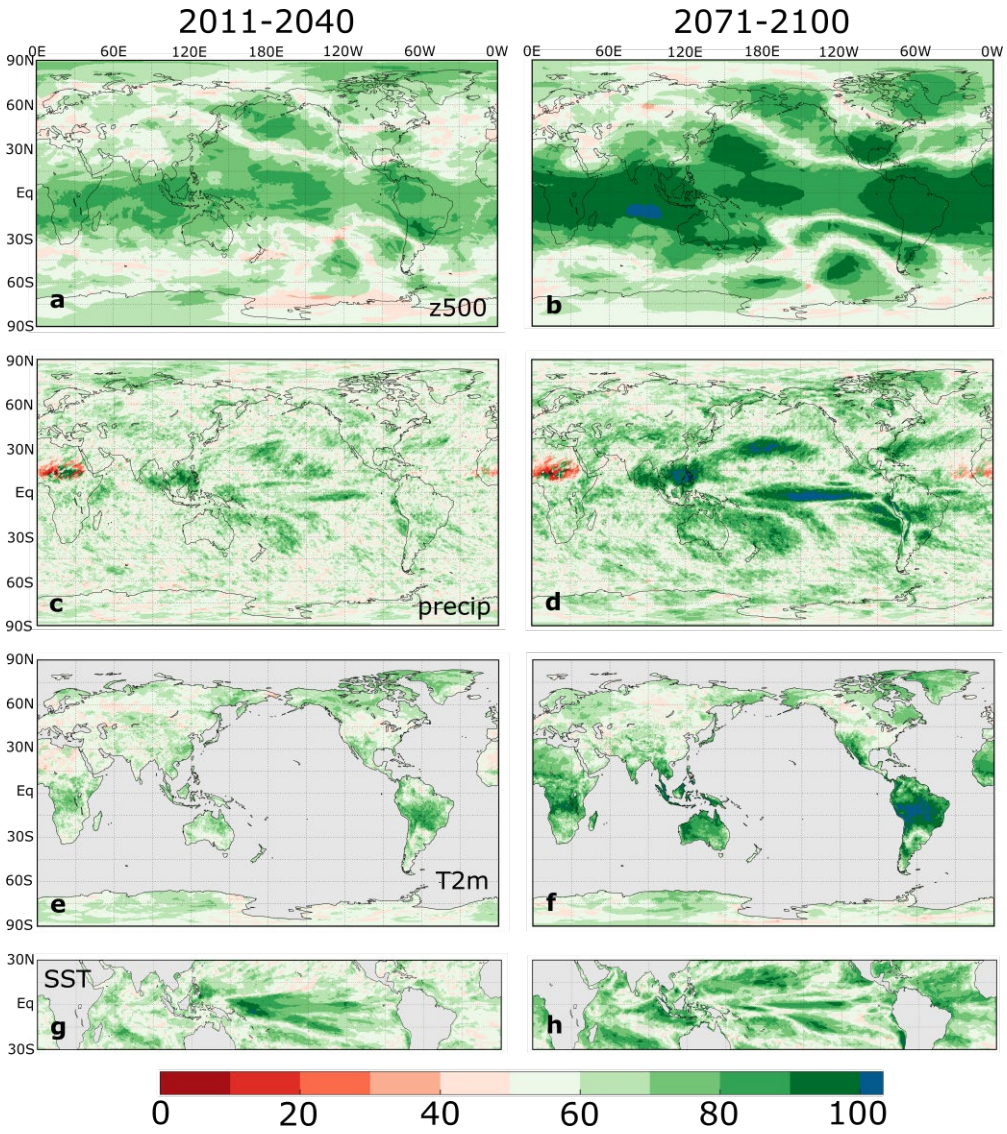

Supplementary Figure 7. Percentage of ensemble members that agree on the ensemble mean SPEAR DJF composite change relative to 1951-1980, as in Fig. 6 but for La Niña instead of El Niño.

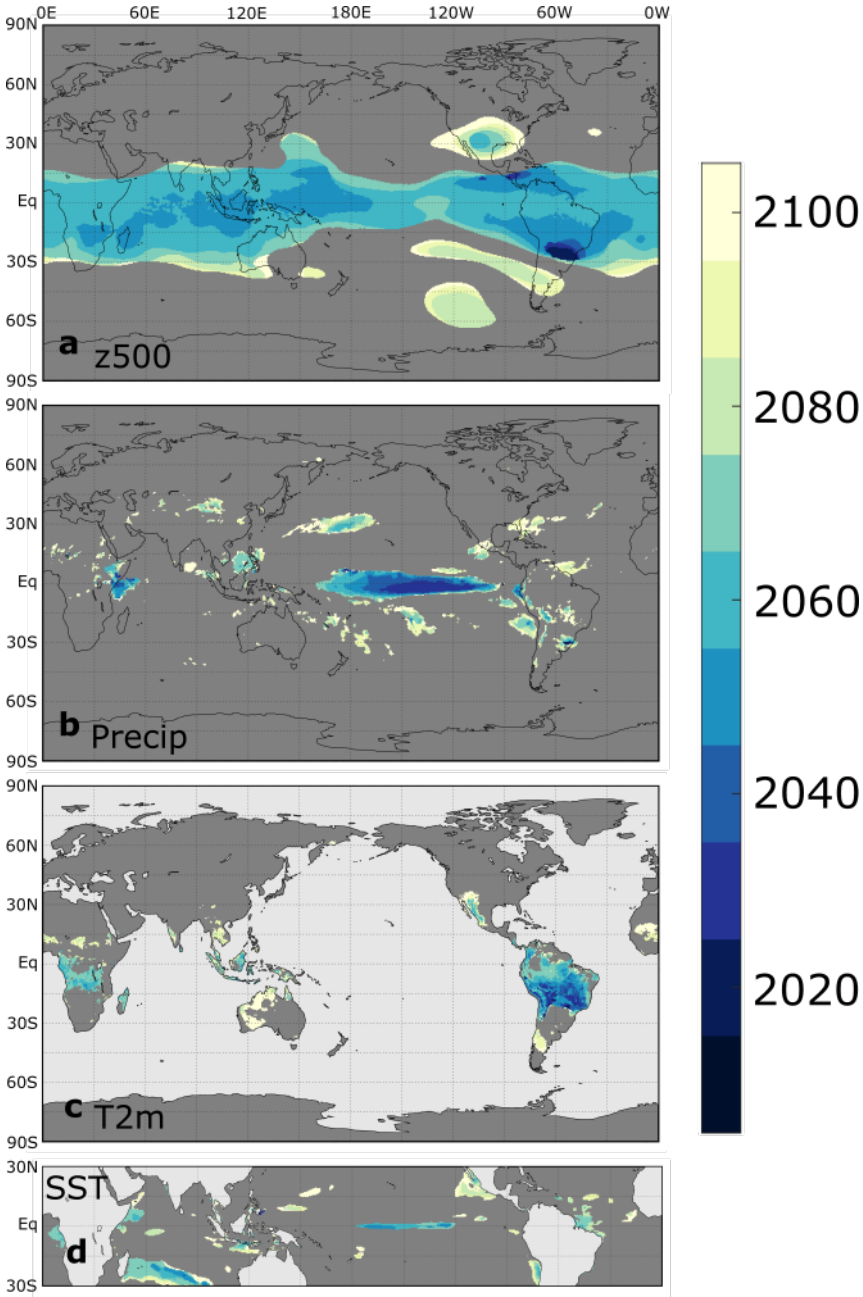

Supplementary Figure 8. DJF teleconnection change time of emergence (ToE) for SSP5-8.5, as in Fig. 7, but for La Niña instead of El Niño.

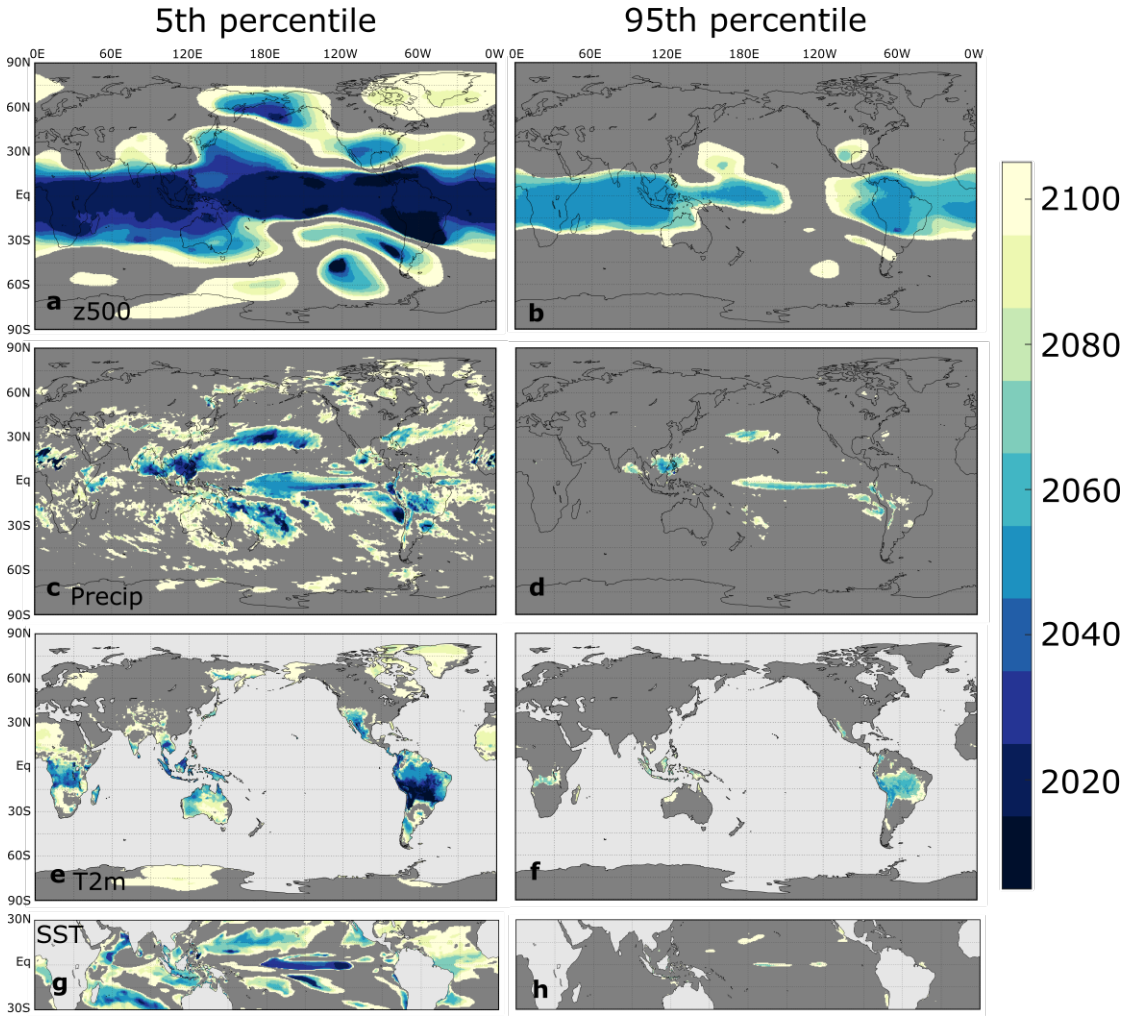

Supplementary Figure 9. Estimated uncertainty of the SSP5-8.5 DJF El Niño teleconnection change time of emergence (ToE), as measured by the (left) 5th and (right) 95th percentiles of the bootstrap ToE distributions (see text for details). The ToE is shown for (a,b) 500 hPa geopotential height, (c,d) precipitation, (e,f) T2m, and (g,h) SST.

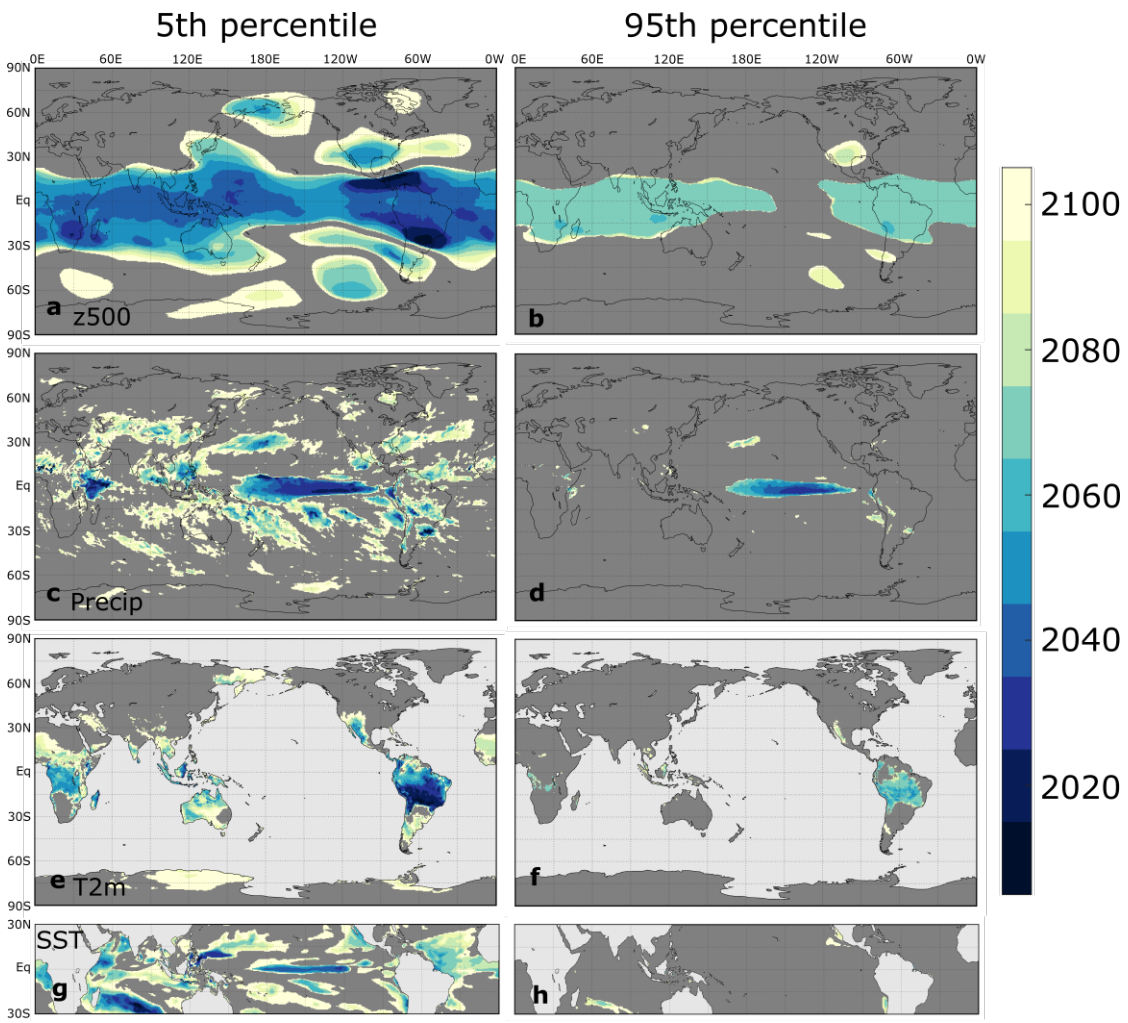

Supplementary Figure 10. As in Supplementary Fig. 8 but for La Niña instead of El Niño.

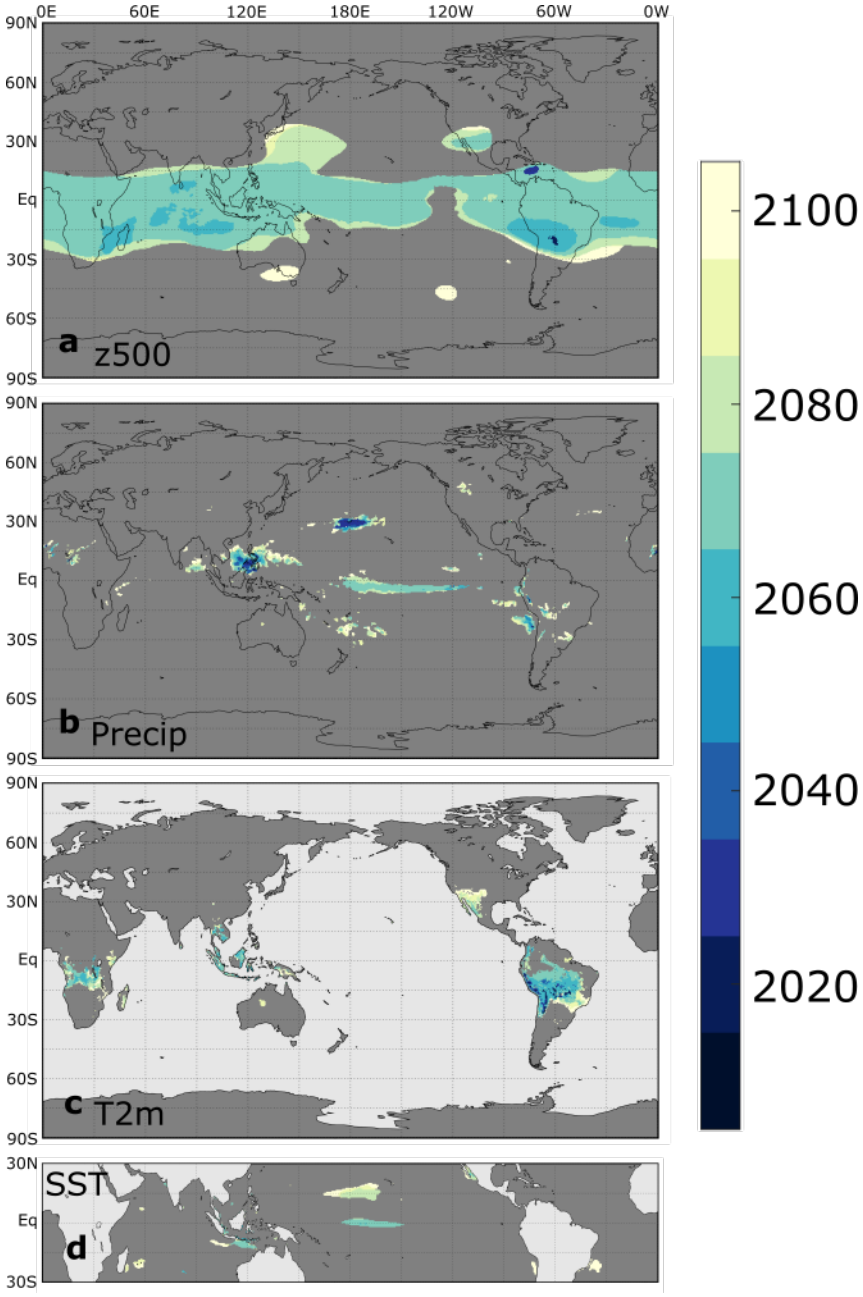

Supplementary Figure 11. DJF El Niño teleconnection change time of emergence (ToE), as in Fig. 7, but for SSP2-4.5 instead of SSP5-8.5.

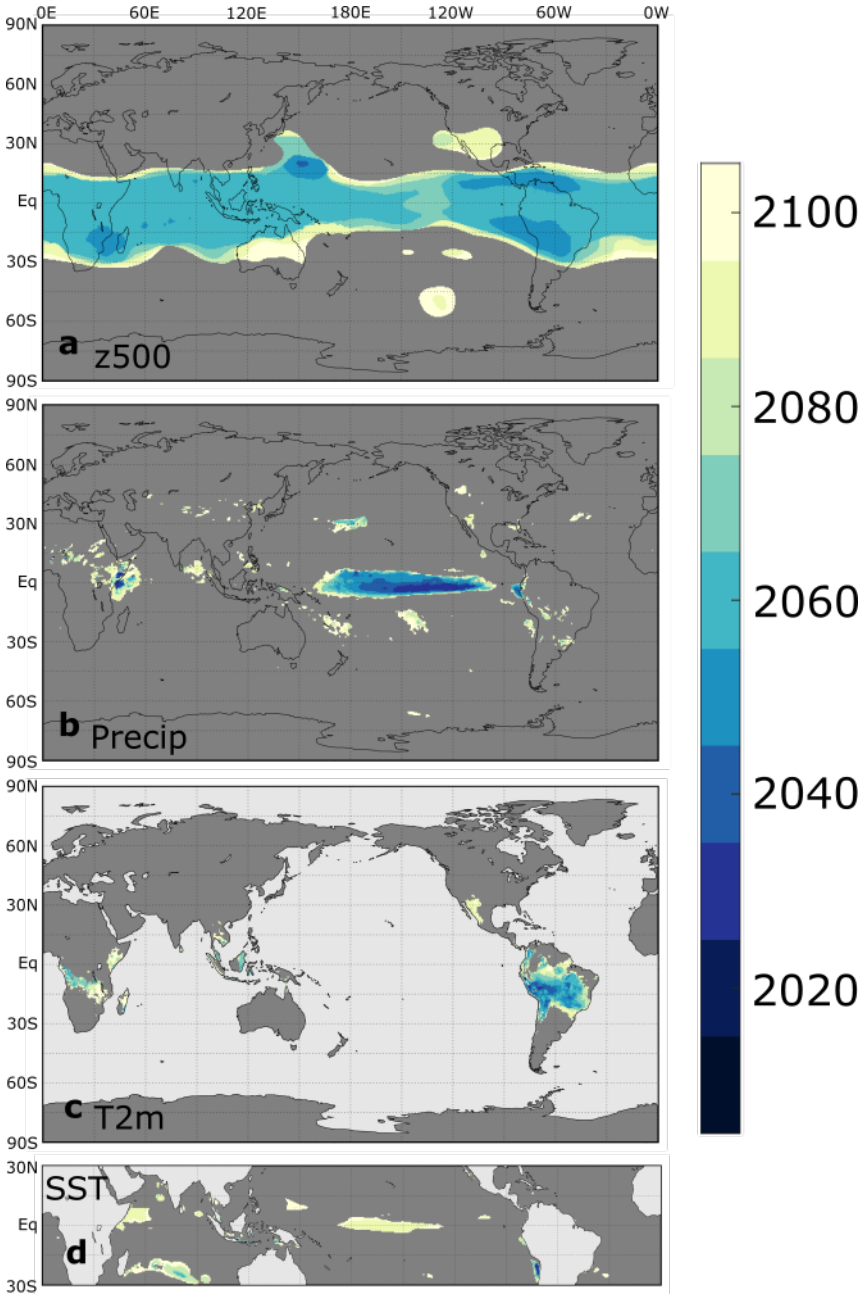

Supplementary Figure 12. DJF teleconnection change time of emergence (ToE), as in Fig. 7, but for La Niña instead of El Niño and SSP2-4.5 instead of SSP5-8.5.

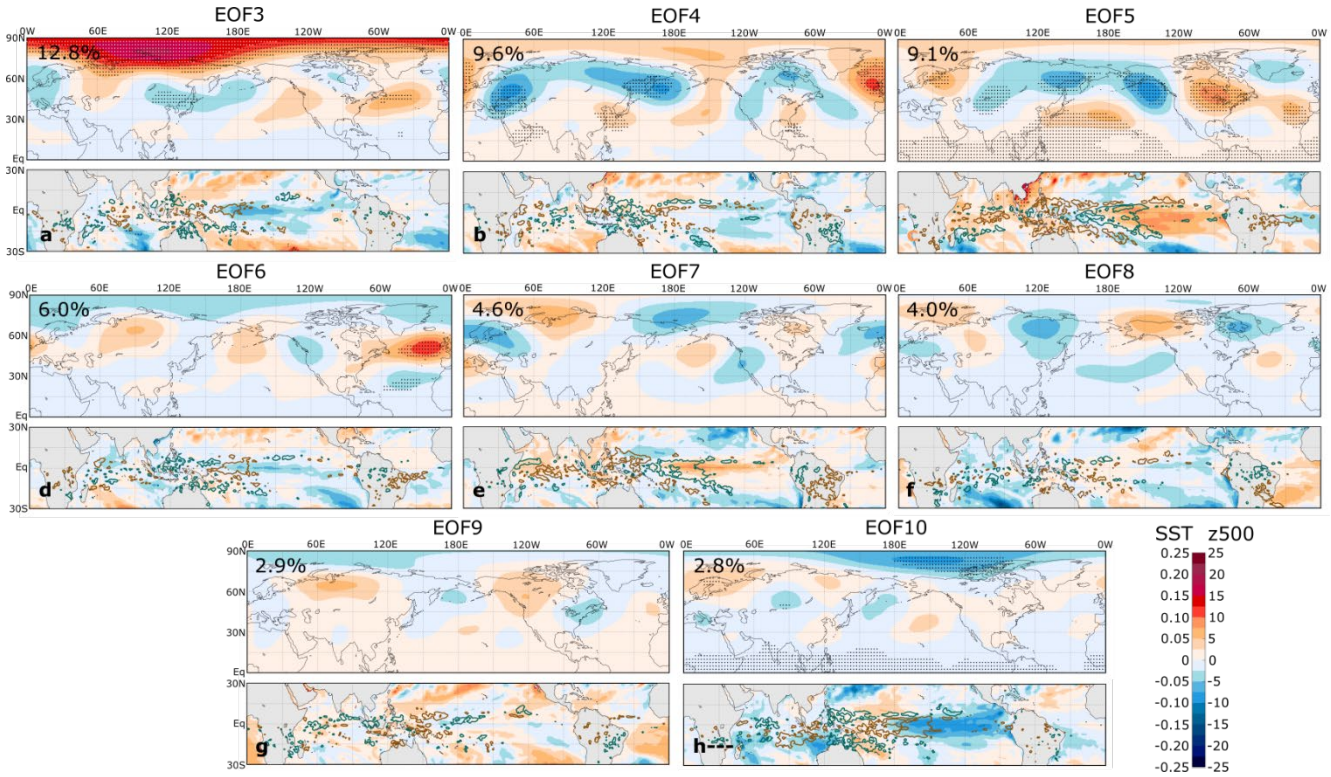

Supplementary Figure 13. Linear regressions of simulated z500 (top panels, color shading, units of m), SST (bottom panels, color shading, units of °C), and precipitation anomalies (bottom panels, green contours at values of 0.2 and 0.5 mm day^{-1} and brown contours at values of -0.2 and -0.5 mm day^{-1}) on the standardized principal components of DJF El Niño 1951-2000 z500 composite anomalies, as in Fig. 8, but for EOFs 3-10.